Supporting Information

Enhanced Electrocatalytic Reduction of CO_2 to Formate via Doping Ce in Bi_2O_3 Nanosheets

Xiao Li,‡[a] Ningkang Qian,‡[a] Liang Ji,[a] Xingqiao Wu,[a] Junjie Li,[a] Jingbo Huang,[a] Yucong Yan,[a,c] Deren Yang,[a] Hui Zhang[a,b,*]

[a]*State Key Laboratory of Silicon Materials and School of Materials Science and Engineering, Zhejiang University, Hangzhou, Zhejiang 310027, People's Republic of China.*

[b]*Institute of Advanced Semiconductors, Hangzhou Innovation Center, Zhejiang University, Hangzhou, Zhejiang 310027, People's Republic of China.*

[c]*BTR New Material Group CO., LTD., GuangMing District, Shenzhen 518106, People's Republic of China*

Corresponding to msezhanghui@zju.edu.cn

‡ These authors contributed equally to this work.

Experimental section

Chemicals

Bismuth (III) nitrate pentahydrate ($Bi(NO_3)_3 \cdot 5H_2O$, 98%) and Cerium(III) nitrate hexahydrate ($Ce(NO_3)_3 \cdot 6H_2O$, 99%) were both purchased from Sigma Aldrich. Potassium bicarbonate ($KHCO_3$, 99.9%) were bought from Macklin Biochemical Co., Ltd. Ethylene glycol and ethanol were purchased from Sinopharm Chemical Reagent Co., Ltd. Ultra-pure deionized (18.2 MΩ·cm) water (DIW) is used in all the aqueous experiments. All the reagents were used without additional purification.

Synthesis of Ce-doped Bi_2O_3 NSs

Ce-doped Bi_2O_3 NSs were synthesized in mixed polyol by a solvothermal method. In a typical procedure, different amounts of $Ce(NO_3)_3 \cdot 6H_2O$ (3.8, 7.6, and 11.4 mg) and 170 mg of $Bi(NO_3)_3 \cdot 5H_2O$ were dissolved in a mixture of 6 mL of ethanol, 3 mL of ethylene glycol and 1 mL DIW, and then sonicated for 30 min. After that, the obtained transparent solution was sealed in a 15 mL Teflon-lined stainless-steel autoclave was heated in an oven at 160 °C for 5 h. Subsequently, the product was centrifuged and washed with ethanol and deionized water for five times. Finally, Ce-doped Bi_2O_3 NSs powder was obtained after freeze-drying.

Synthesis of undoped Bi_2O_3 Nanosheets

The Bi_2O_3 NSs were prepared by the similar procedure as Ce-doped Bi_2O_3 NSs, except for no $Ce(NO_3)_3 \cdot 6H_2O$ adding in the solvothermal synthesis.

Characterizations of Materials

The X-ray diffraction (XRD) measurement was performed on the X-ray diffractometer (Rigaku D/max-ga) with Cu Kα radiation (graphite monochromatized, λ = 1.541 Å). The atomic ratio of Bi and Ce in these samples were analyzed by inductively coupled plasma atomic emission spectrometry (ICP-AES, IRIS Intrepid II XSP, TJA Co.). Transmission electron microscopy (TEM) images were taken on a Hitachi HT-7700 microscope and the operating voltage is 100 kV. A FEI Tecnai G2 F20 microscope was employed to achieve high-resolution (HRTEM) images operated at 200 kV accelerating voltage. High-angle annular dark-field scanning TEM (HAADF-STEM) images were

taken on a FEI Titan ChemiSTEM whose operating voltage is 200 kV. X-ray photoelectron spectrometer (XPS) analysis was carried out on a scanning X-ray microprobe (Axis Supra, Kratos Inc.) with Al Kα radiation. Each binding energies in this paper was calibrated with C-C 1s peak (284.8 eV). CO_2 adsorption isotherms were obtained by Micromeritics ASAP 2020M at 25°C. Two cycles of gas desorption were performed before the experiment.

Electrochemical measurements

Electrochemical testing was carried out in a home-made H-type two-compartment cells. The cathode compartment housed the working electrode, reference electrode (Ag/AgCl) and the gas inlet and outlet. The anode compartment housed the counter electrode (2 cm × 2 cm Pt plate). To prepare the working electrode, 1 mg of catalyst powder and 0.5 mg of carbon black (XC-72R) were dispersed in 125 μL ethanol,125 μL of DIW and 10 μL of 5 wt% Nafion solution, and bath-sonicated for 0.5 h to form a homogeneous ink. The ink was then uniformly spread on a 1 cm × 1 cm carbon fiber paper and dried naturally. Each one of the two compartments was filled with 35 mL of 0.5 M $KHCO_3$ electrolyte and the two parts were separated by an anion exchange membrane. The aforementioned electrolyte was bubbled with CO_2 for 1 h prior to measurements. During the ECR measurements, the electrolyte was continuously bubbled with CO_2 at a flow rate of 20 sccm. In the cathodic compartment, the electrolyte is under stirring with a stir bar at a mild speed. All the potentials mentioned below were converted to RHE using this equation: $E_{RHE} = E_{Ag/AgCl} + 0.197 + 0.0591 \times pH$ and none of the potentials have been IR-corrected. Electroreduction products were qualitatively and quantitatively analyzed using online-gas chromatography (Agilent, GC7980B) and ion chromatography (Beijing Liyuan, EP-1000D). The faradic efficiency (FE) for gas products (H_2 or CO) was calculated as follows:

$$FE_{H_2 \text{ or } CO}(\%) = \frac{Q_{H_2}}{Q_{total}} \times 100\% = \frac{(\frac{v}{60\ s/min}) \times (\frac{y}{24000 cm^3/mol}) \times N \times F}{i} \times 100\%$$

where v = 20 sccm, which is the CO_2 flow rate, y is the product concentration measured

by GC, N = 2 is the number of electron transfer to form a molecule of H_2 or CO, F is the Faraday constant (96485 C·mol^{-1}), and i is the total current measured by the electrochemical workstation (CHI760E). The FE for formate in the catholyte was calculated as follows:

$$FE_{HCOO^-}(\%) = \frac{Q_{HCOO^-}}{Q_{total}} \times 100\% = \frac{n_{HCOO^-} \times N \times F}{Q} \times 100\%$$

where n_{HCOO^-} is the amount of formate determined by ion chromatography, and the Q corresponds to the amount of cumulative charge in the process of CO_2 reduction, which was provided by the electrochemical workstation. The energy efficiency (EE) at a certain negative potential for formate generation was calculated as follows:

$$EE = \frac{E_0 \times FE}{E_0 + \eta} \times 100\%$$

Where E_0 (V) is the difference between the standard half reaction potentials for water oxidation (1.23 V vs RHE) and the reduction of CO_2 into HCOOH (-0.2 V vs RHE); FE (%) is the faradic efficiency for formate generation at the equilibrium potential; η (V) is the overpotential, that is the difference between the working potential at the cathode and the reduction of CO_2 into HCOOH (-0.2 V vs RHE).

The ECSA of all the electrocatalysts is estimated from the electrochemical double-layer capacitance (C_{dl}), which is derived from the cyclic voltammograms (CVs) at a non-Faradaic potential range (0.13 V vs. RHE to 0.23 V vs. RHE). The CV scan rates are from 20 mV/s to 200 mV/s.

DFT calculation details.

The first-principles calculations were carried out with the Vienna ab initio simulation package[1,2]. The interaction between ions and valence electrons is described using projector augmented wave (PAW) potentials, and the exchange-correlation between electrons is treated through using the generalized gradient approximation (GGA) in the Perdew-Burke-Ernzerhof (PBE) form[3]. To achieve the accurate density of the electronic states, the plane wave cutoff energy was 500 eV, a 3× 3×1 for sheet k-point mesh were used. Ionic relaxations were carried out under the conventional energy (10-

^{4} eV) and force (0.01 eV/Å) convergence criteria. The Bi_2O_3 slab along the (200) projection was used to mimic the as-prepared (200) lattice plane, in which 15 Å vacuum layer was added to avoid the interaction between adjacent layers.

Gibbs free energies for each gaseous and adsorbed species were calculated at 298.15 K, according to the expression:

$G = E_{DFT} + E_{ZPE} - TS$

$E_{ZPE} = \sum_i 1/2\ h\nu_i$

$\Theta_i = h\nu_i / k$

$S = \sum_i R[\ln (1-e^{-\Theta i/T})^{-1} + \Theta_i/T\ (e^{\Theta i/T} - 1)^{-1}]$

where E_{DFT} is the electronic energy calculated for specified geometrical structures, E_{ZPE} is the zero-point energy, S is the entropy, h is the Planck constant, ν is the computed vibrational frequencies, Θ is the characteristic temperature of vibration, k is the Boltzmann constant, and R is the molar gas constant. For adsorbates, all 3N degrees of freedom were treated as frustrated harmonic vibrations with negligible contributions from the catalysts' surfaces. In the computational hydrogen electrode (CHE) model,[4] each reaction step was treated as a simultaneous transfer of the proton-electron pair as a function of the applied potential.

The adsorption energy (E_{ads}) of the OCHO was calculated as $E_{ads} = E_{substrate+adsorbate} - E_{substrate} - E_{adsorbate}$.

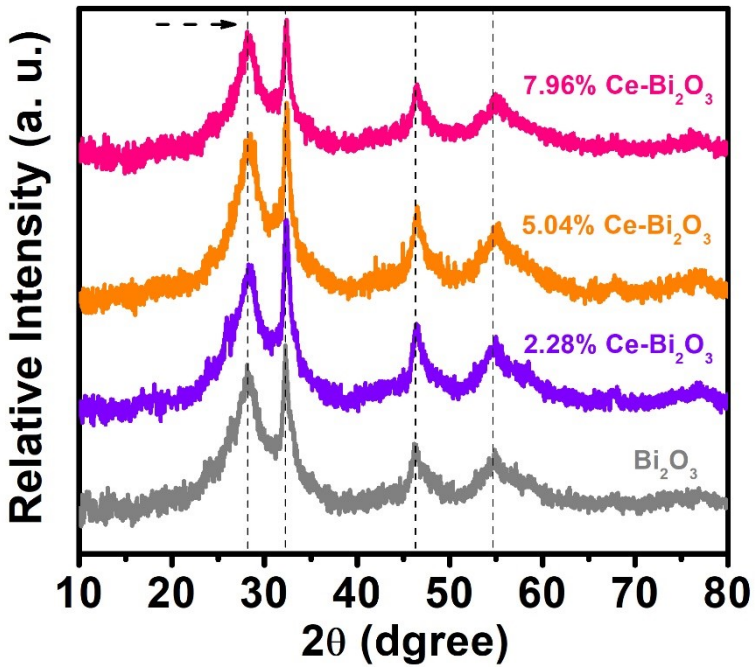

Fig. S1. XRD patterns of undoped Bi_2O_3 NSs, 2.28% Ce-doped Bi_2O_3 NSs, 5.04% Ce-doped Bi_2O_3 NSs and 7.96% Ce-doped Bi_2O_3 NSs.

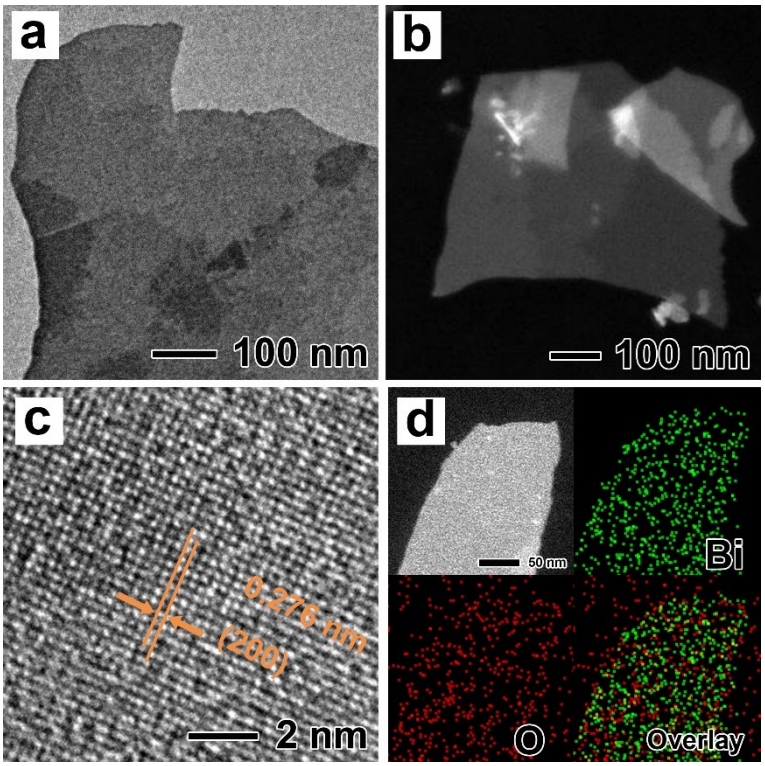

Fig. S2. (a) TEM, (b) HAADF-STEM, (c) HRTEM, and (d) elemental mapping images of undoped Bi_2O_3 NSs.

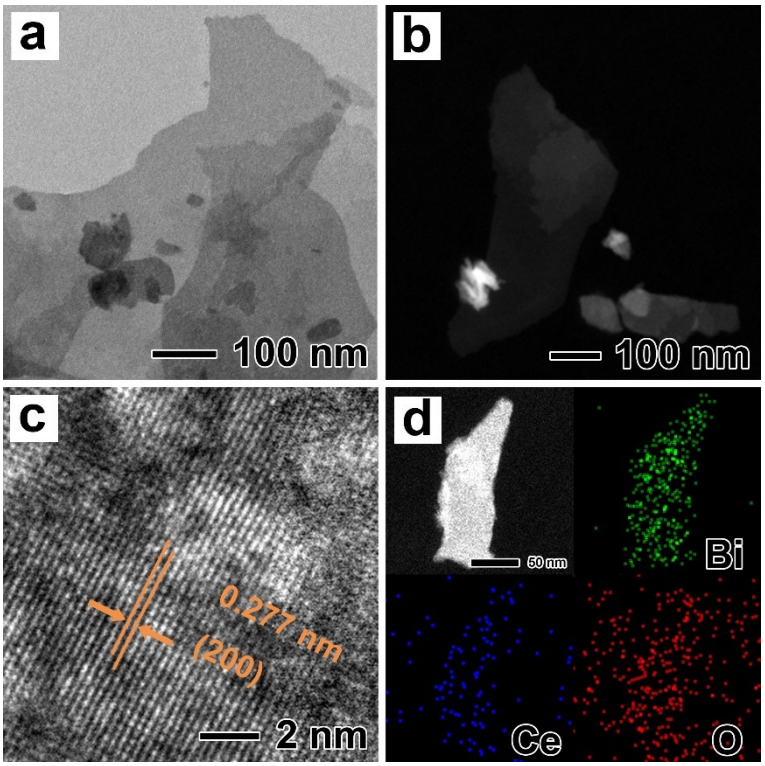

Fig. S3. (a) TEM, (b) HAADF-STEM, (c) HRTEM, and (d) elemental mapping images of 2.28% Ce-doped Bi_2O_3 NSs.

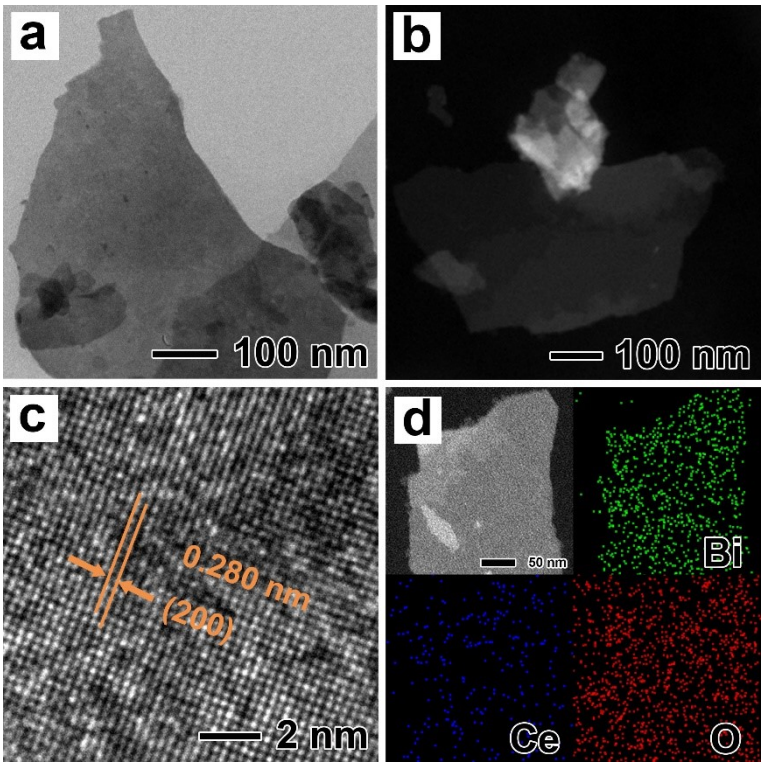

Fig. S4. (a) TEM, (b) HAADF-STEM, (c) HRTEM, and (d) elemental mapping images of 7.96% Ce-doped Bi_2O_3 NSs.

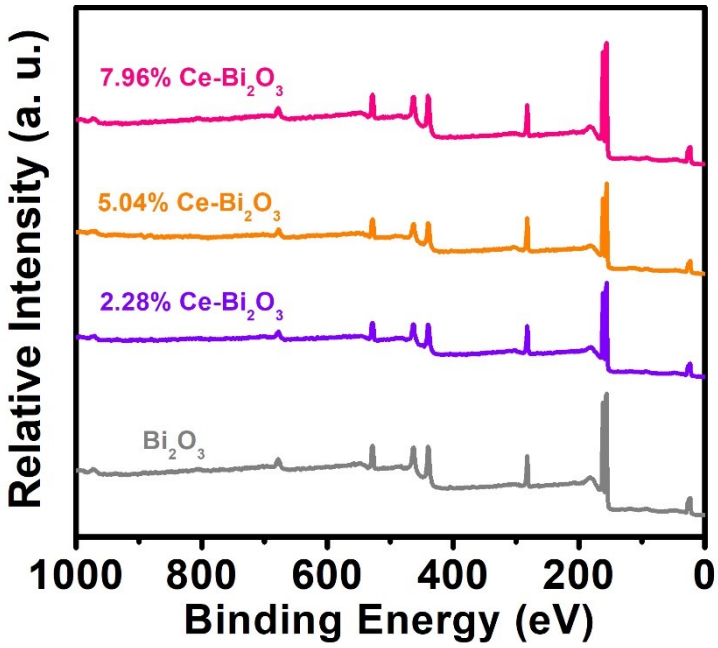

Fig. S5. The survey XPS spectra for undoped Bi_2O_3 NSs, 2.28% Ce-doped Bi_2O_3 NSs, 5.04% Ce-doped Bi_2O_3 NSs and 7.96% Ce-doped Bi_2O_3 NSs.

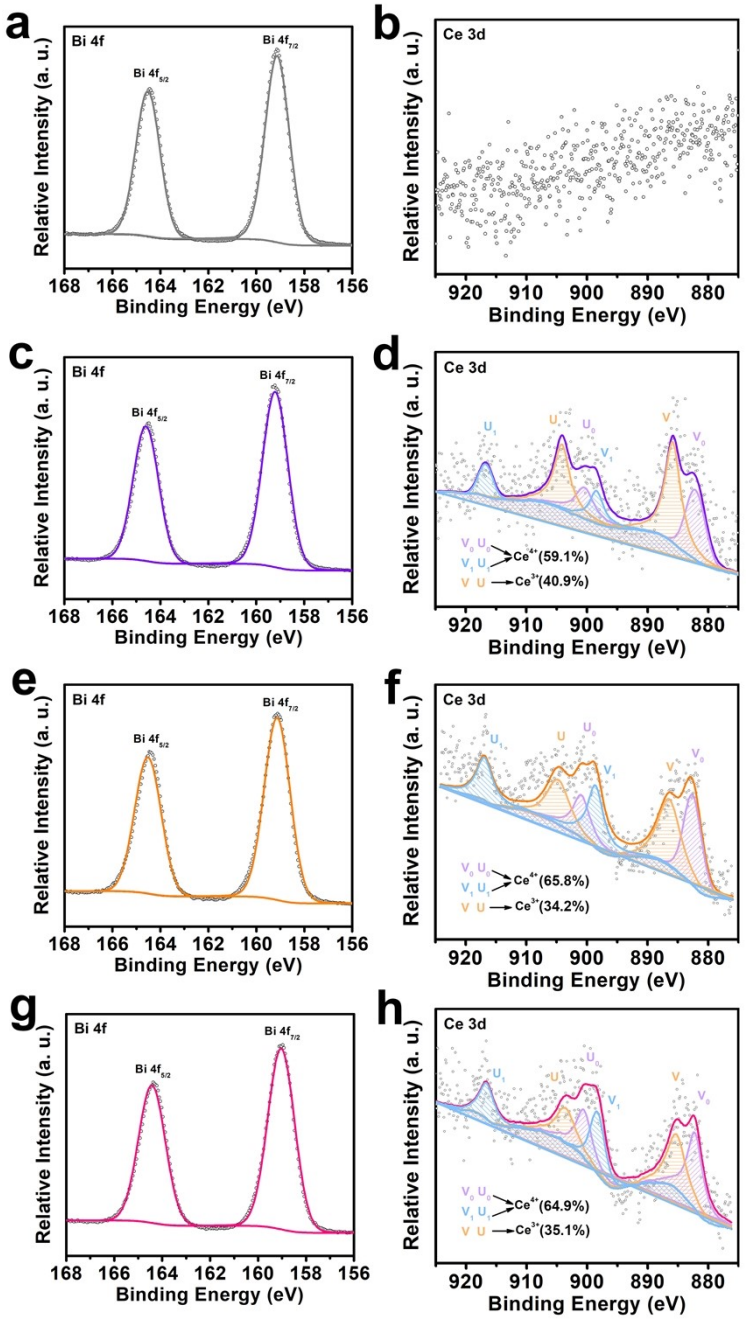

Fig. S6. XPS spectra of (a) Bi 4f orbitals and (b) Ce 3d orbitals for undoped Bi_2O_3 NSs, 2.28% Ce-doped Bi_2O_3 NSs, 5.04% Ce-doped Bi_2O_3 NSs and 7.96% Ce-doped Bi_2O_3 NSs.

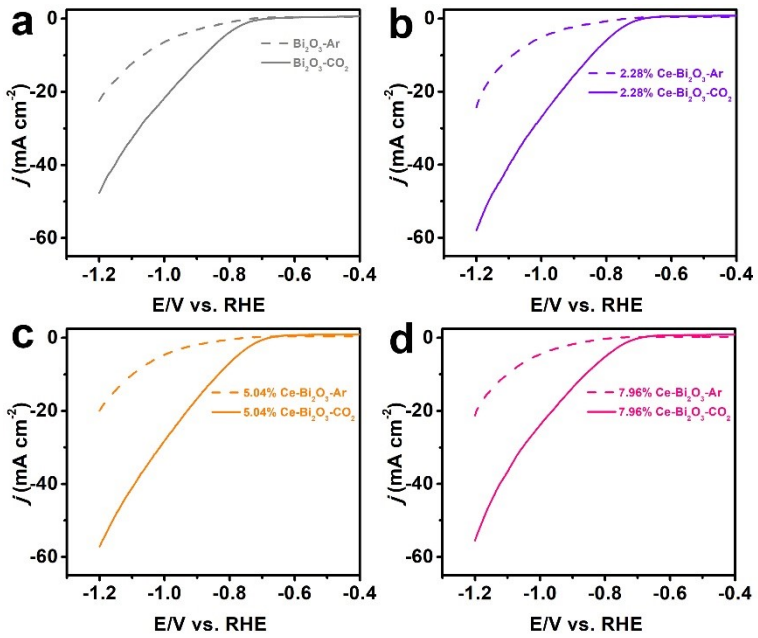

Fig. S7. Linear sweep voltammogram curves performed in Ar-saturated and CO_2-saturated 0.5 M $KHCO_3$ for (a) undoped Bi_2O_3 NSs, (b) 2.28% Ce-doped Bi_2O_3 NSs, (c) 5.04% Ce-doped Bi_2O_3 NSs and (d) 7.96% Ce-doped Bi_2O_3 NSs.

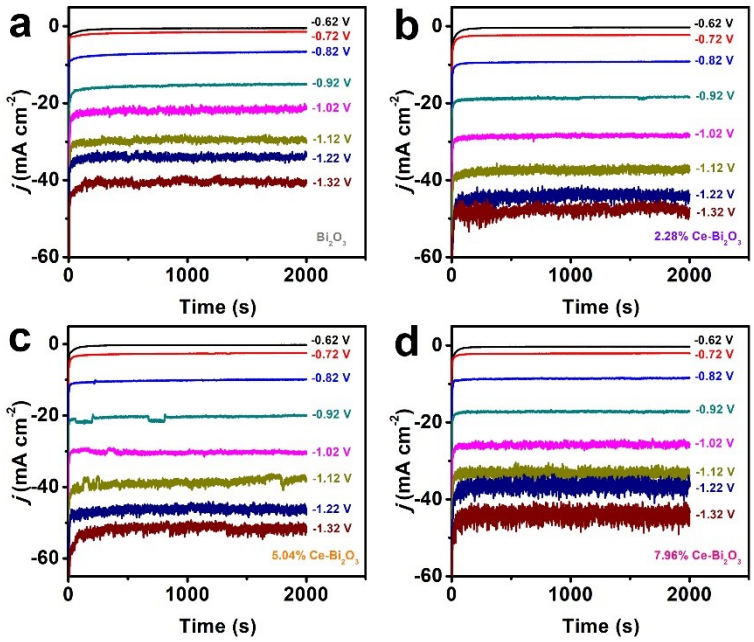

Fig. S8. Plots of current densities *j* as a function of time (chronoamperograms) during ECR at different cathodic potentials for (a) undoped Bi_2O_3 NSs, (b) 2.28% Ce-doped Bi_2O_3 NSs, (c) 5.04% Ce-doped Bi_2O_3 NSs and (d) 7.96% Ce-doped Bi_2O_3 NSs.

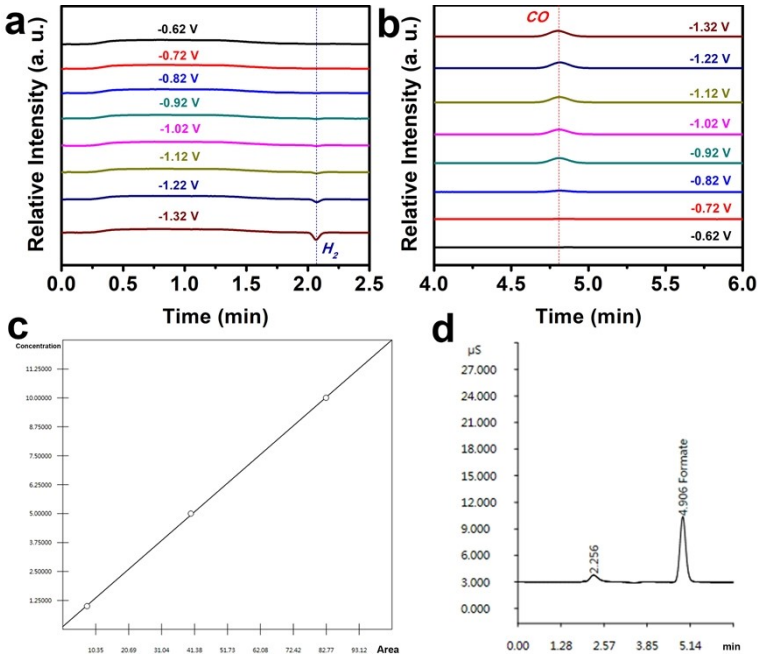

Fig. S9. The outflow curves of (a) H_2 and (b) CO obtained by gas chromatography for 5.04% Ce-doped Bi_2O_3 NSs at different cathodic potentials. (c) The standard curve of formic acid ($HCOO^-$) and (d) ionic chromatography spectrum of the electrolyte obtained after 2000 s electrolysis at -1.12 V of the 5.04% Ce-doped Bi_2O_3 NSs.

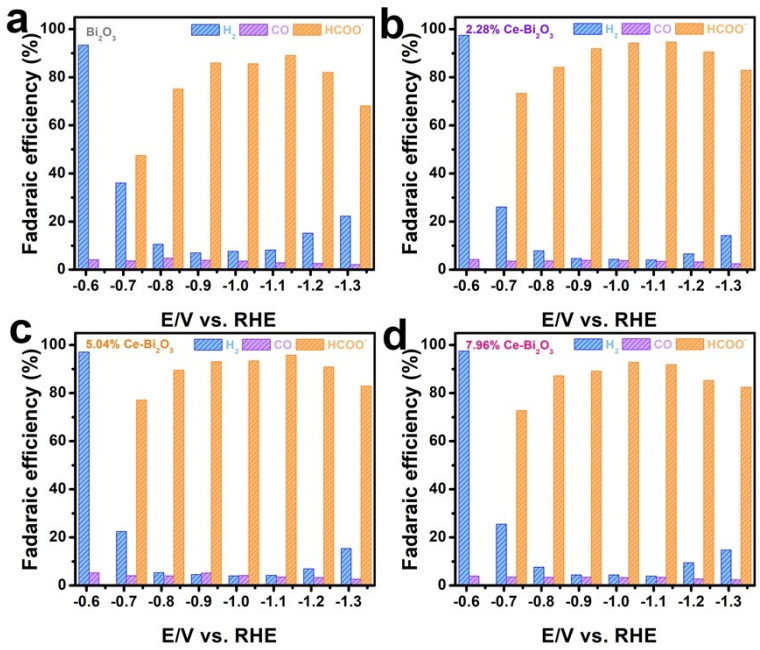

Fig. S10. Potential-dependent FEs of $HCOO^-$, CO, and H_2 for (a) undoped Bi_2O_3 NSs, (b) 2.28% Ce-doped Bi_2O_3 NSs, (c) 5.04% Ce-doped Bi_2O_3 NSs and (d) 7.96% Ce-doped Bi_2O_3 NSs.

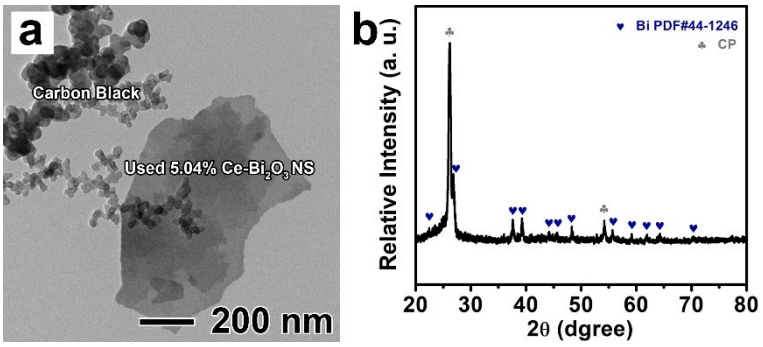

Fig. S11. (a) TEM image and (b) XRD pattern of 5.04% Ce-doped Bi_2O_3 NSs after stability test.

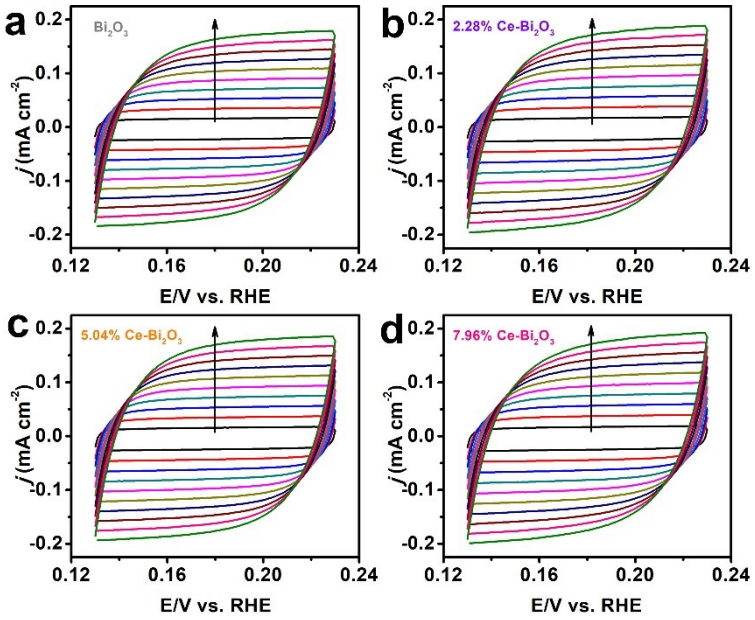

Fig. S12. Typical cyclic voltammetry curves of (a) undoped Bi_2O_3 NSs, (b) 2.28% Ce-doped Bi_2O_3 NSs, (c) 5.04% Ce-doped Bi_2O_3 NSs and (d) 7.96% Ce-doped Bi_2O_3 NSs at different scan rates (20 mV/s to 200 mV/s).

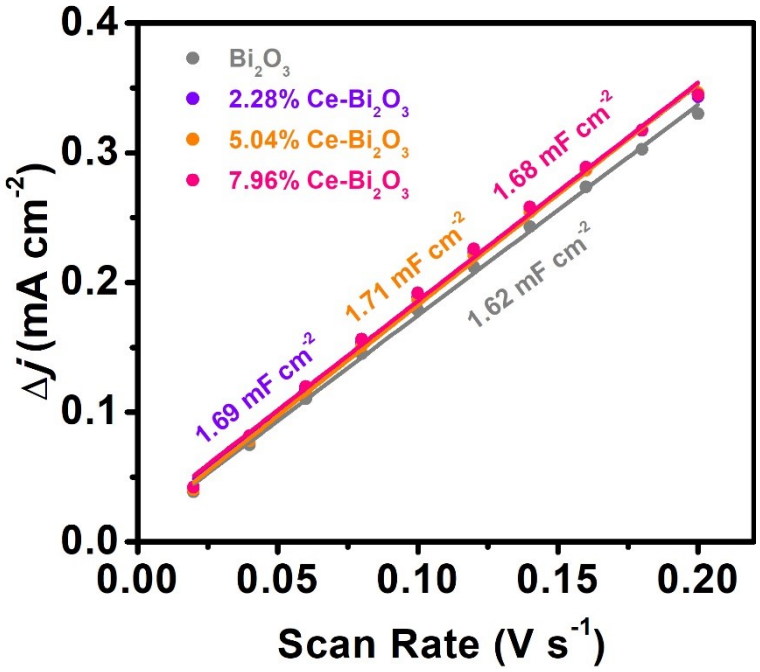

Fig. S13. Linear fitting of double-layer capacitive currents Δj *vs.* scan rates of undoped Bi_2O_3 NSs, 2.28% Ce-doped Bi_2O_3 NSs, 5.04% Ce-doped Bi_2O_3 NSs and 7.96% Ce-doped Bi_2O_3 NSs.

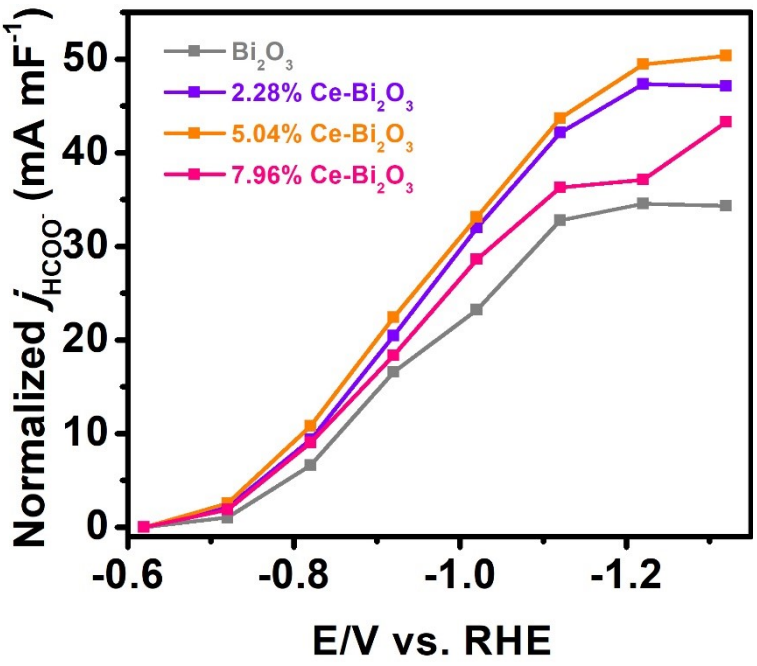

Fig. S14. The j_{HCOO^-} normalized by the C_{dl} value of undoped Bi_2O_3 NSs, 2.28% Ce-doped Bi_2O_3 NSs, 5.04% Ce-doped Bi_2O_3 NSs and 7.96% Ce-doped Bi_2O_3 NSs.

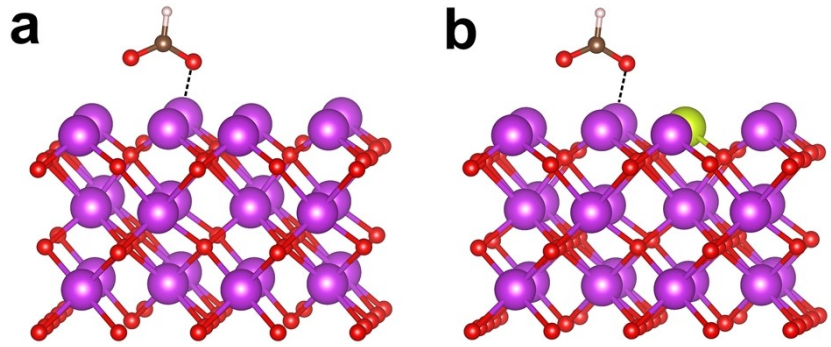

Fig. S15. DFT optimized adsorption configurations for $OCHO^*$ on (a) undoped Bi_2O_3 and (c) Ce-doped Bi_2O_3 (Purple, yellow-green, red, brown, and pink balls represent Bi, Ce, O, C, and H atoms, respectively).

Table S1 Comparison of the ECR activity with state-of-the-art Bi-based electrocatalysts in H-cell.

Catalyst	FE(%) @ (V vs. RHE)	Formate Current density (mA cm^{-2}) @ (V vs. RHE)	Reference
Bi NS	95 (-0.87)	14.1 (-0.87)	[5]
Bi NSs	86 (-1.1)	14.2 (-1.1)	[6]
Bi NS	93 (-0.97)	23 (-0.97)	[7]
mesoporous Bi NSs	99 (-0.9)	17 (-1)	[8]
BiO_x/C	93.4 (-1.12)	16.1 (-1.12)	[9]
Bi_2O_3	91 (-0.9)	8 (-0.9)	[10]
Bi_2O_3NSs/NCF	94.1 (-1)	16.9 (-1)	[11]
Bi_2O_3NSs@MCCM	93.8 (-1.256)	17.73 (-1.356)	[12]
Bi_2O_3-NGQDs	98.1 (-0.9)	18.1 (-0.9)	[13]
Bi/Bi_2O_3	90.4 (-0.87)	38.8 (-0.87)	[14]
Bi/Bi_2O_3/NrGO	85 (-0.9)	18 (-0.9)	[15]
Bi/CeO_x	92 (-1.3)	137 (-1.3)	[16]
S-Bi_2O_3-CNT	97.06 (-0.9)	28.17 (-0.9)	[17]
Boron-doped Bi	95 (-0.9)	24.7 (-1.2)	[18]
5.04% Ce-doped Bi_2O_3 NSs	**95.8 (-1.12)** **83 (-1.32)**	**37.4 (-1.12)** **43.1 (-1.32)**	**This work**

Reference

[1] G. Kresse, J. Furthmuller, *Comp. Mater. Sci.*, 1996, **6,** 15-50.

[2] Y. Surendranath, M. W. Kanan, D. G. Nocera, *J. Am. Chem. Soc.*, 2010, **132,** 16501-16509.

[3] J. P. Perdew, K. Burke, M. Ernzerhof, *Phys. Rev. Lett.*, 1997, **78,** 1396-1396.

[4] A. A. Peterson, F. A. Pedersen, F. Studt, J. Rossmeisl, J. K. Nørskov, *Energy Environ. Sci.*, 2010, **3,** 1311.

[5] N. Han, Y. Wang, H. Yang, J. Deng, J. Wu, Y. Li, Y. Li, *Nat. Commun.*, 2018, **9,** 1320.

[6] W. Zhang, Y. Hua, L. Ma, G. Zhu, P. Zhao, X. Xue, R. Chen, S. Yang, J. Ma, J. Liu, Z. Jin, *Nano Energy*, 2018, **53,** 808-816.

[7] D. Wu, X. Shen, J. Liu, C. Wang, Y. Liang, X. Fu, J. Luo, *Nanoscale*, 2019, **11,** 22125.

[8] H. Yang, N. Han, J. Deng, J. Wu, Y. Wang, Y. Hu, P. Ding, Y. Li, Y. Li, J. Lu, *Adv. Energy Mater.*, 2018, **8,** 1801536.

[9] C. W. Lee, J. S. Hong, K. Yang, K. Jin, J. H. Lee, H. Y. Ahn, H. Seo, N. E. Sung, K. T. Nam, *ACS Catal.*, 2018, **8,** 931-937.

[10] P. Deng, H. Wang, R. Qi, J. Zhu, S. Chen, F. Yang, L. Zhou, K. Qi, H. Liu, B. Xia, *ACS Catal.*, 2020, **10,** 743-750.

[11] F. Meng, Q. Zhang, K. Liu, X. Zhang, *Chem. Eur. J.*, 2020, **26,** 4013-4018.

[12] S. Liu, X. Lu, J. Xiao, X. Wang, X. Lou, *Angew. Chem. Int. Ed.*, 2019, **58,** 1-7.

[13] Z. Chen, K. Mou, X. Wang, L. Liu, *Angew. Chem. Int. Ed.*, 2018, **57,** 12790-12794.

[14] D. Wu, G. Huo, W. Chen, X. Fu, J. Luo, *Appl. Catal. B Environ.*, 2020, **271**, 118957.

[15] J. Sun, W. Zheng, S. L. Lyu, F. He, B. Yang, Z. Li, L. Lei, Y. Hou, *Chinese Chem. Lett.*, 2020, **31,** 1415-1421.

[16] Y. Duan, Y. Zhou, Z. Yu, D. Liu, Z. Wen, J. Yan, and Q. Jiang, *Angew. Chem. Int. Ed.*, 2021, **60**, 8798-8802.

[17] S. Liu, M. Gao, R. Feng, L. Gong, H. Zeng, and J. Luo, *ACS Catal.*, 2021, **11**, 7604-7612.

[18] X. Chen, H. Chen, W. Zhou, Q. Zhang, Z. Yang, Z. Li, F. Yang, D. Wang, J. Ye, and L. Liu, *Small*, 2021, **17**, 2101128.